Inter J Nav Archit Oc Engng (2009) 1:20~28
http://dx.doi.org/10.2478/IJNAOE-2013-003

Three dimensional numerical simulations for non-breaking solitary wave interacting with a group of slender vertical cylinders

Weihua Mo[1] and Philip L.-F. Liu[1,2]

[1]School of Civil and Environmental Engineering, Cornell University, Ithaca, NY, USA
[2]Institute of Hydrological and Oceanic Sciences, National Central University, Taiwan

ABSTRACT: *In this paper we validate a numerical model for wave-structure interaction by comparing numerical results with laboratory data. The numerical model is based on the Navier-Stokes (N-S) equations for an incompressible fluid. The N-S equations are solved by a two-step projection finite volume scheme and the free surface displacements are tracked by the volume of fluid (VOF) method. The numerical model is used to simulate solitary waves and their interaction with a group of slender vertical piles. Numerical results are compared with the laboratory data and very good agreement is observed for the time history of free surface displacement, fluid particle velocity and wave force. The agreement for dynamic pressure on the cylinder is less satisfactory, which is primarily caused by instrument errors.*

KEY WORDS: Three dimensional simulation; Volume of fluid (VOF) method; Non-breaking solitary wave; Interaction; Slender vertical cylinders

INTRODUCTION

Vertical cylinders are among the most commonly used structures in coastal and offshore engineering. In the nearshore region they are used for jetties or piers and in deepwater for offshore platforms and windmill farms. In designing these structures, it is critical to be able to calculate wave forces acting on each individual cylinder and, in some cases, a group of cylinders. For a slender cylinder, where the diameter of the cylinder (D) is small in comparison with the design wavelength (λ), the Morison formula (Morison, O'Brien, Johson and Schaaf 1950) is a good approximation for calculating the wave forces. On the other hand, if the diameter of the cylinder or the distance between two adjacent cylinders is not sufficiently small, the presence of cylinders will generate significant scattered waves and the wave forces can be accurately calculated only if the interaction between waves and cylinders is fully considered (Sapkaya and Issacson 1981).

Information on wave forces can be obtained by means of laboratory experiments or numerical simulations. Even when the Morison formula is used, the dependency of two coefficients, C_D (drag coefficient) and C_M (mass coefficient), on the design wave conditions and the geometry of the cylinder must be determined based on the experimental data or numerical simulations. Since laboratory experiments are usually constrained by the physical dimensions of the laboratory facilities, it is not very always feasible to perform extensive parameter studies (e.g., variation of water depth, diameter and inclination of cylinders, wave parameters, breaker type, and configuration of cylinders in a group) even if the costs are of no concern. The alternative is to use numerical simulations as supplements to laboratory experiments. In other words, a limited numbers of experiments can be designed so that the laboratory data are effectively used to validate numerical models. The validated numerical models can then be used to simulate scenarios with much wider range of physical parameters of interest. Moreover, accurate numerical simulations will also provide much more detailed insights into the physical processes that could not be achieved by experimental approach.

Modeling the interaction between waves and a group of cylinders faces multiple challenges similar to other wave-structure interaction problems. First of all, the flow is complex and three-dimensional. The free surface runs up and down on the cylinders. For large incident waves, breaking might occur in front of cylinders and flow separation on the lee side of the cylinders. Therefore, local, but strong turbulence in the vicinity of the cylinder and near the free surface need to be considered. So far, most of the numerical models developed for three-dimensional wave propagation have been built upon the potential flow theory. For instance, using integral equation methods, highly accurate numerical models have been developed for wave propagation over

Corresponding author: *Philip L. -F. Liu*
e-mail: *pll3@cornell.edu*

varying bathymetry in shallow water and for wave-body interaction in deep water (Xue, Xu, Liu and Yue 2001; Liu, Xue and Yue 2001; Guyenne and Grilli 2006). However, the potential flow assumption limits these models' applications to irrotational flow.

Three-dimensional Euler's equations or Navier-Stokes (N-S) equations must be employed to describe rotational flows. Theoretically, the direct numerical simulation (DNS) can always be performed to resolve the entire spectrum of motions ranging from large eddy motions to the smallest turbulence (Kolmogorov) scale motions. Clearly, the DNS requires very fine spatial and temporal resolutions and most of DNS applications can only be applied to relatively low Reynolds number flows within a small computational domain (Kim, Moin, and Moser 1987). With the currently available computing resources, the DNS is still not a feasible approach for investigating wave-structure interaction problems if wave breaking and flow separation are important.

The alternatives to the DNS approach for computing the turbulent flow characteristics include the Reynolds Averaged Navier-Stokes (RANS) equations method and the Large Eddy Simulation (LES) method. In the RANS equations method, only the ensemble-averaged (mean) flow motion is resolved. The turbulence effects appear in the momentum equations for the mean flow and are represented by the Reynolds stresses, which are often modeled by an eddy viscosity model. The eddy viscosity can be further modeled in several different closure models (Pope 2001). For example in the $k-\varepsilon$ closure model, the eddy viscosity is hypothesized as a function of the turbulence kinetic energy (TKE, k) and the turbulence dissipation rate (ε), for which balance equations are constructed semi-empirically. Lin and Liu (1998) have successfully applied the $k-\varepsilon$ turbulence model in their studies of wave breaking and runup in the surf zone, in which the mean flow is primarily two dimensional. Lin and Liu's model has been extended and applied to many different coastal engineering problems, including the wave-structure interaction (e.g., Liu, Lin and Chang 1999).In the LES method, the three-dimensional turbulent motions are directly simulated and resolved down to a pre-determined scale, and the effects of smaller-scale motions are then modeled by closures, which are still not well understood for complex flows (Pope 2004). In terms of the computational expense, LES lies between RANS and DNS. Compared to DNS in solving high-Reynolds-number flows, LES avoids explicitly representing small-scale motions and therefore, the computational costs can be greatly reduced. Compared to RANS models, because the large-scale unsteady motions are computed explicitly, LES can be expected to provide more statistical information for the turbulence flows in which large-scale unsteadiness is significant (Pope 2001, 2004).

The flow governing equations for LES are filtered N-S equations by applying a low-pass spatial filter. Similar to the RANS approach, a term related to the residual-stress tensor or the sub-grid-scale (SGS) Reynolds stress tensor appears in the filtered N-S equations. Thus, a closure model is also required to relate the residual-stress tensor to the filtered velocity field. The traditional Smagorinsky model (Smagorinsky 1963) is probably the simplest LES-SGS model and has been used in several breaking wave studies Watanabe and Saeki 1999; Lin and Li 2002; Christensen and Deigaard 2001; Liu, Wu, Raichlen, Synolakis and Borrero 2005). Recently, Mo, Irschik, Oumeraci and Liu (2007) applied the model developed by Liu et al. (2005), which was originally designed for studying landslide generated tsunamis, to calculate the wave forces acting on a single slender pile, in which the breaking is insignificant. On the other hand, using the same model, Wu and Liu (2009b) calculated the impact forces acting on a vertical cylinder by a broken bore. The LES model as also described in Wu and Liu (2009a) solves the filtered NS equations using a two-step projection algorithm with finite volume formulation. The Volume-of-Fluid (VOF) method (Hirt and Nichols 1981) is employed to track free surface motions. The Smagorinsky SGS model is employed in the model.

The main objective of the present paper is to check first whether the core algorithms of the model (i.e., the VOF method and the two-step projection methods) are adequate for dealing with the interaction between waves and a group of cylinders. Since the available experimental data are for non-breaking solitary waves, we will ignore the viscous and turbulent effects in the original model and focus only on the Euler's equations without any dissipative mechanism. The laboratory data sets, containing large-scale measurements of the water surface elevation, the fluid particle velocity, the pressure at different locations around the circumference of the cylinders and total wave forces are used to check the accuracy of the numerical model.

THE NUMERICAL MODEL

Fluid motions of incompressible and inviscid fluid can be described by the Euler's equations:

$$\nabla \cdot \mathbf{u} = 0 \tag{1}$$

$$\frac{\partial \mathbf{u}}{\partial t} + \nabla \cdot (\mathbf{u}\mathbf{u}) = -\frac{1}{\rho}\nabla p + \mathbf{g} \tag{2}$$

where $\mathbf{u}$ represents velocity vector, ρ water density, $\mathbf{g}$ the gravity force vector, t time, and P pressure.

On the free surface, the dynamic boundary condition requires that the pressure field be zero. On the other hand, the kinematic boundary condition is replaced by requiring the conservation of a volume of fluid function, f, representing the volume fraction of water within a computational cell. The f value equals to one, if the cell is full, zero if empty, and $0<f<1$ if the cell is partially filled with water, representing a free surface cell. The governing equation for f can be described by:

$$\frac{\partial f}{\partial t} + \nabla \cdot (f\mathbf{u}) = 0 \tag{3}$$

The Euler's equations are solved by the two-step projection method (Hirt and Nichols 1981). The momentum equations, (2), are split into two fractional steps:

$$\frac{\rho^{n+1}\mathbf{u}^{*}-\rho^{n}\mathbf{u}^{n}}{\Delta t}=-\nabla\cdot\left(\rho^{n}\mathbf{uu}\right)^{n} \quad (4)$$

$$\frac{\rho^{n+1}\mathbf{u}^{n+1}-\rho^{n+1}\mathbf{u}^{*}}{\Delta t}=-\nabla p^{n+1}+\rho^{n+1}\mathbf{g} \quad (5)$$

in which the superscript "n" denotes the n-th time step. Equation (4) is an explicit expression for the interim velocity, $\mathbf{u}^{*}$, referred to as the predictor step. On the other hand, (5) is called the projection step. Combining (4) with (5) produces the time discretization of Equation (2):

$$\frac{\rho^{n+1}\mathbf{u}^{n+1}-\rho^{n}\mathbf{u}^{n}}{\Delta t}=-\nabla\cdot\left(\rho\mathbf{uu}\right)^{n}-\nabla p^{n+1}+\rho^{n+1}\mathbf{g} \quad (6)$$

No additional approximation results from this decomposition. Equation (5) relates $\mathbf{u}^{n+1}$ to $\mathbf{u}^{*}$. By adopting the continuity condition, (1), we have:

$$\nabla\cdot\frac{\nabla p^{n+1}}{\rho^{n+1}}=\nabla\cdot\left(\frac{\mathbf{u}^{*}}{\Delta t}+\mathbf{g}\right) \quad (7)$$

The above equation is also called the Poisson Pressure Equation (PPE). The pressure p^{n+1} at the new time step can be obtained by solving (2.7). The two-step projection method is implemented in a finite volume algorithm so that unstructured computational grids (cells) can be used. We also note that a multidimensional PLIC (Piecewise Linear Interface Calculation) method (Rider and Kothe 1998) is utilized to construct the free surface. The details of the algorithm can be found in Wu and Liu (2009b).

COMPARISON OF LABORATORY DATA AND NUMERICAL RESULTS

To check the capability and accuracy of our current numerical model, numerical simulations of non-breaking solitary waves and their interaction with a group of three vertical cylinders were conducted and the results were compared with the experiments conducted in the Tsunami Wave Basin at the O. H. Hinsdale Wave Research Laboratory (WRL) of the Oregon State University (OSU).

Laboratory Set-Up in the OSU Experiments

The wave basin at the WRL of OSU has an effective length of 160 ft (48.8 m), a width of 87 ft (26.5 m) and a depth of 7 ft (2.1 m). Stainless steel circular cylinders with a diameter, D, of 4 ft (1.219 m) were instrumented and installed in the basin. This paper deals only with a series of experiments of non-breaking solitary waves with either one or three cylinders being placed on flat bottom of the basin. A sketch of the placement of these cylinders is shown in Fig. 1.

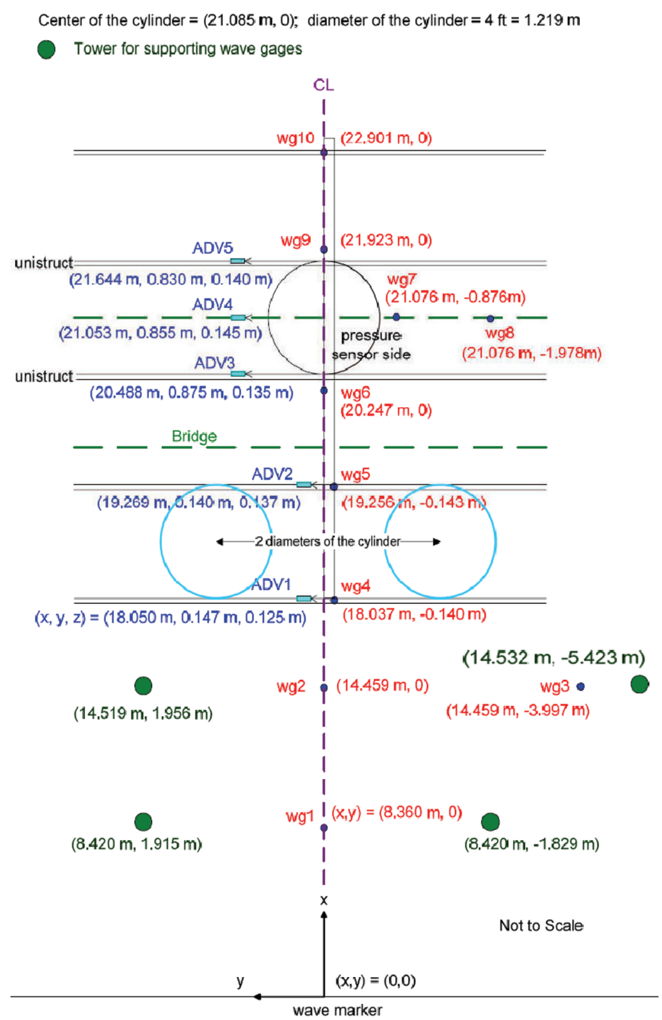

Fig. 1 A sketch of the locations of cylinders, instruments and wave-maker.

The wave basin at the WRL of OSU has an effective length of 160 ft (48.8 m), a width of 87 ft (26.5 m) and a depth of 7 ft (2.1 m). Stainless steel circular cylinders with a diameter, D, of 4 ft (1.219 m) were instrumented and installed in the basin. This paper deals only with a series of experiments of non-breaking solitary waves with either one or three cylinders placed on flat bottom of the basin. A sketch of the placement of these cylinders is shown in Fig. 1. For the one-cylinder experiments, those two cylinders closer to the wave maker are removed. To measure wave characteristics 10 wave gauges and 5 Acoustic Doppler Velocimetries (ADVs) were deployed. Their locations are also indicated in Figure 1. Additionally, 47 pressure transducers were fixed on the cylinder, which is farthest from the wave maker. As sketched in Figure 2 the pressure transducers are uniformly distributed along the frontline of the cylinder with spacing $\triangle z = 0.1m$ and are also spread out over the circumference in four horizontal cross sections. In this paper two representative experimental cases (one cylinder and three cylinders) are used to check the numerical results in detail. In both cases the still water depth is fixed at $h = 0.75m$ and the wave height of the solitary wave take the value of $H = 0.3m$. In the first case with one cylinder, the cylinder with pressure transducers remains in place.

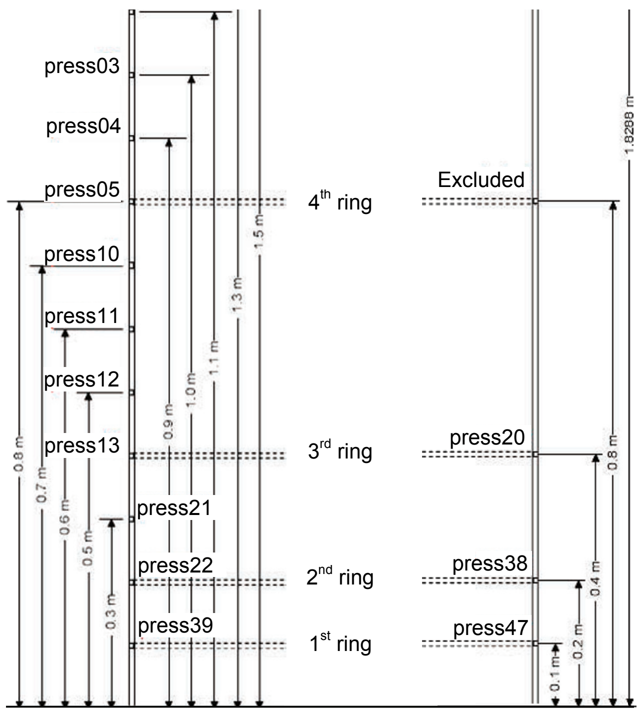

Fig. 2 A sketch of the locations of pressure transducers on the cylinder.

Numerical simulations of OSU solitary wave experiments

The numerical simulations were performed only in a half of the wave basin because of the symmetric arrangement of the locations for cylinders and the computational resource constraint. The origin of the coordinate system is located on the incident boundary, with $z = 0$ indicating the bottom of the basin. The length of the computational region in the direction of wave propagation in front of the cylinders is one wavelength that contains 95% of the total mass of the incident solitary wave. The lateral domain length is 3D or 5D for the case of single cylinder and the case of three cylinders, respectively, to ensure that the reflection from the lateral wall has not reached the cylinders at the end of each numerical simulation.

The upper (ceiling) and lower (bottom of the wave basin) boundaries and two lateral boundaries as well as the surface of the cylinders of the computational domain are rigid boundaries. Therefore, the no-flux (free slip) boundary condition is applied. The incident wave information, including the velocity and the free surface displacement, are provided from the experimental data at the upstream boundary, while a numerical sponge layer is appended at the end of numerical wave tank to damp out the outgoing wave. Unstructured meshes (finite volumes) are used to discretize the computational domain with smaller volumes in the vicinity of the cylinders. Generally speaking, the volume size is chosen such that there are 60 to 120 grids within one wavelength in the horizontal directions, $L/\triangle x=O(60\sim120)$ and 15 to 20 grids within the wave height in the vertical direction, $H/\triangle x=O(15\sim20)$, where L denotes the wavelength and H the wave height. The total cell number is 568,854 and 1,469,795 for single-cylinder case and three-cylinder case, respectively. The mesh used for the three-cylinder simulation is shown in Fig. 3.

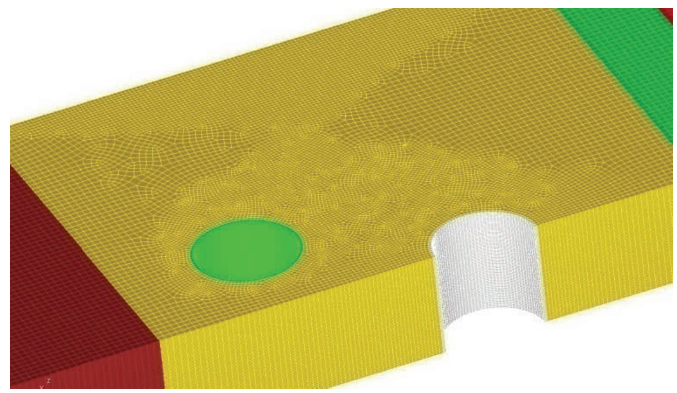

Fig. 3 The three-dimensional mesh for numerical simulations.

The experimentally measured time history of free surface displacements at the wave gauge #1 located at 8.36 m from the wave maker (see Fig. 1) was used as the input incident wave boundary condition at the upstream boundary. The corresponding fluid velocity for the incident wave is calculated using the following approximate formula (Goring and Raichlen 1980):

$$\frac{u}{\sqrt{gh}} = \frac{\eta}{h}\left[\frac{H}{h}+3\left(\frac{H}{h}\right)^2\left(\frac{1}{6}-\frac{1}{2}\left(\frac{z}{h}+1\right)^2\right)\right] - \left(\frac{H}{h}\right)^2\left(\frac{7}{4}-\frac{9}{4}\left(\frac{z}{h}+1\right)^2\right)\left(\frac{\eta}{h}\right)^2 \tag{8}$$

$$\frac{w}{\sqrt{gh}} = \sqrt{\frac{3H}{h}}\left(\frac{z}{h}+1\right)\frac{\eta}{h}\tanh\left(\sqrt{\frac{3H}{4h^3}}\left(x-Ct\right)\right) \times\left\{1+\frac{H}{2h}\left[1-7\frac{\eta}{H}-\left(\frac{z}{h}+1\right)^2\left(1-\frac{3\eta}{H}\right)\right]\right\} \tag{9}$$

where η denotes the measured time history of free surface elevation, H the wave height, h the water depth.

Figure 4 shows the numerical results for the time histories of free surface displacements at several wave gauge locations. In these plots the free surface displacement is normalized by H while the time is scaled by $\sqrt{h/g}$. Excellent agreement between the numerical results and the experimental data is observed for the leading waves at all locations. However, some noticeable differences appear for the secondary scattered waves, which could be the consequence of flow separation.

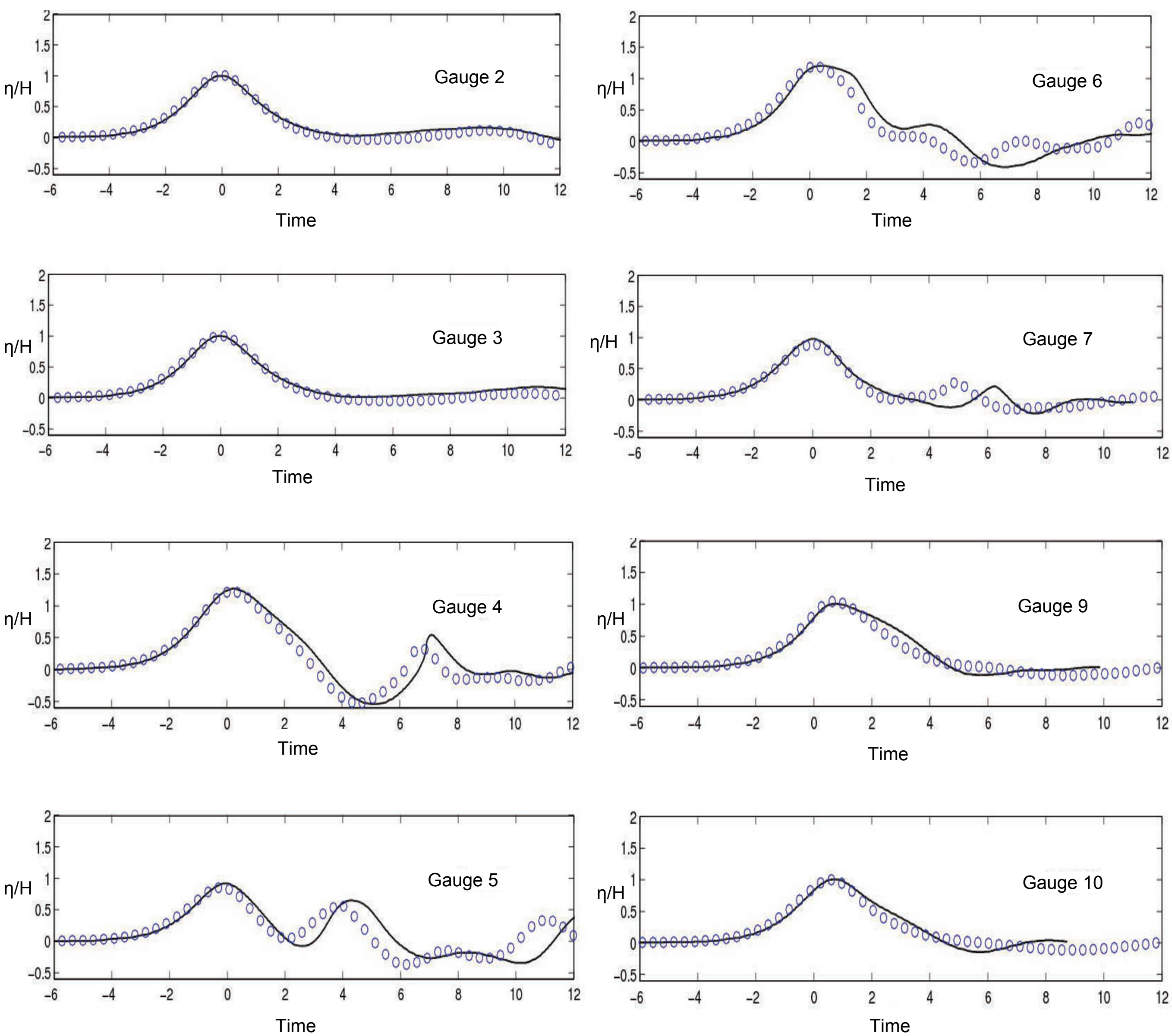

Fig. 4 Time histories of free surface displacements at all wave gauges. The circles are experimental data and the solid lines are numerical results.

Fig. 5 shows the time histories of particle velocity components at different locations. ADV velocity meters are installed at different location as shown in Figure 1. The agreement between the experimental data and the numerical results for all three velocity components is quite good. It is not surprising the flow filed is dominated by the velocity component in the direction of wave propagation, since solitary wave is a long wave. It is interesting to observe that although the second wave crest (due to the wave scattering) appeared in the free surface measurements at wave gage #5 shown in Fig. 4 these oscillations disappeared in the horizontal velocity measurements by ADV2 shown in Fig. 5. The dynamic pressure responses along the front line of the cylinder are shown in Fig. 6. The positions of the pressure transducers can be found in Fig. 2.

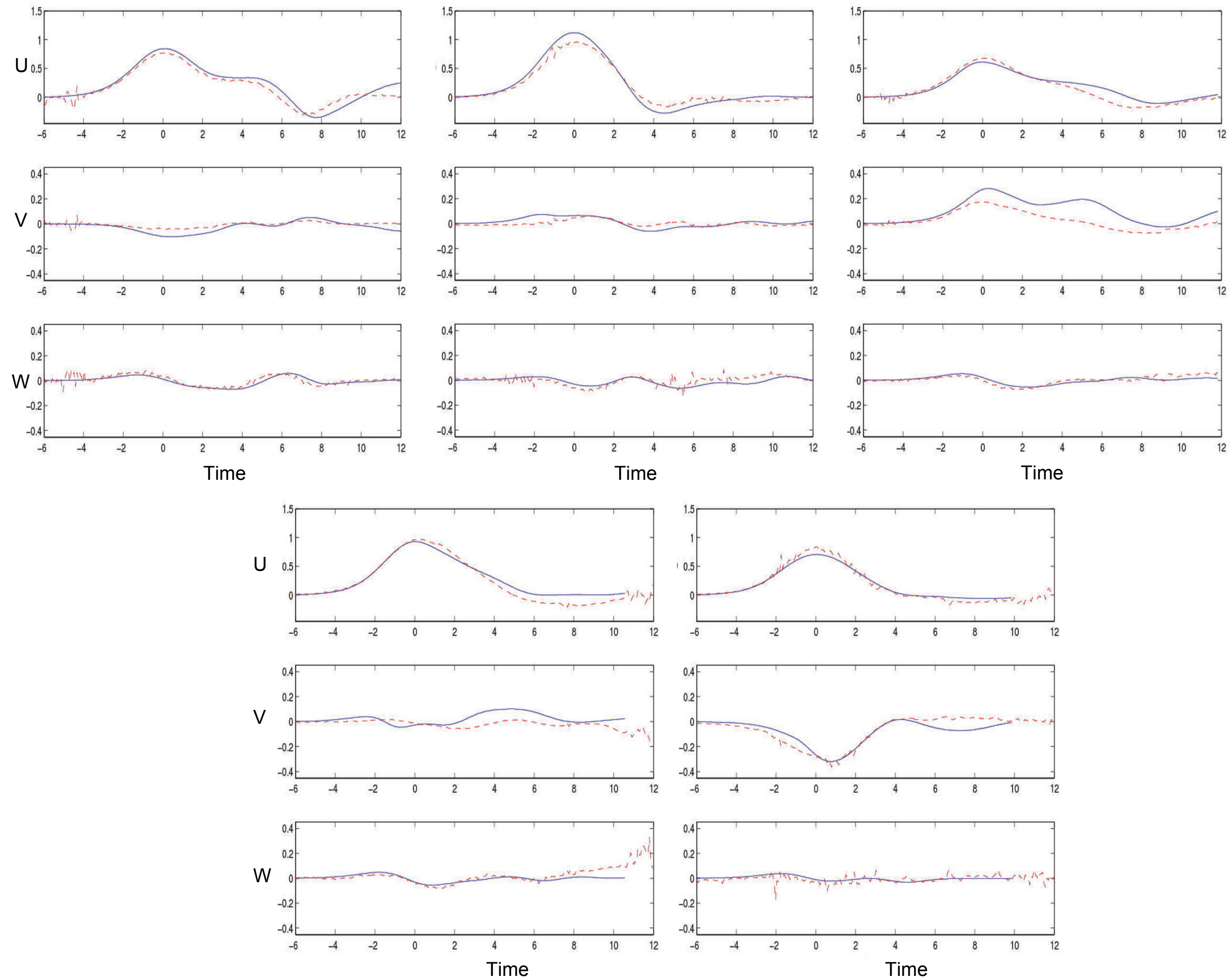

Fig. 5 Time histories of particle velocity components at different ADV locations starting from the upper left panel as ADV1 and ending at the lower right panel as ADV5. The dashed lines are experimental data and the solid lines are numerical results.

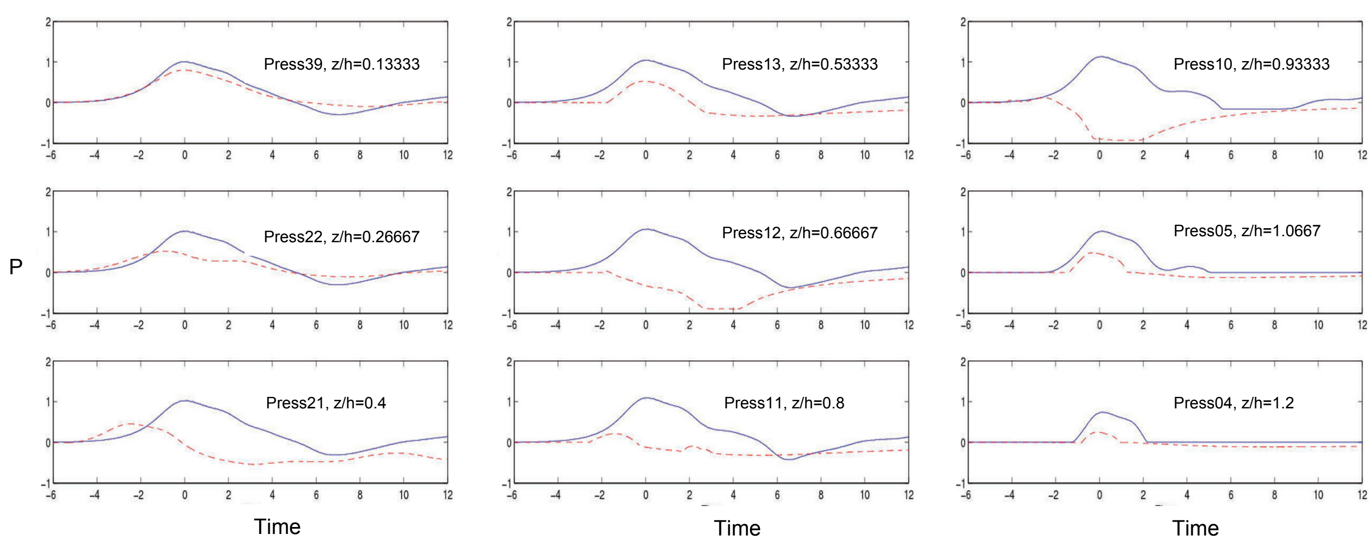

Fig. 6 Time histories of dynamic pressure along the front line of the cylinder. The positions of the pressure transducers can be found in Fig. 2.

The numerical results for the vertical pressure profile along the front face of the cylinder at the wave crest phase are also sown in Fig. 7. The agreement between the numerical results and experimental data is rather disappointing. The measured data are not reasonable at several transducers. For example negative pressures are measured under wave crest at transducer 10. It suggests that some of these transducers did not function properly.

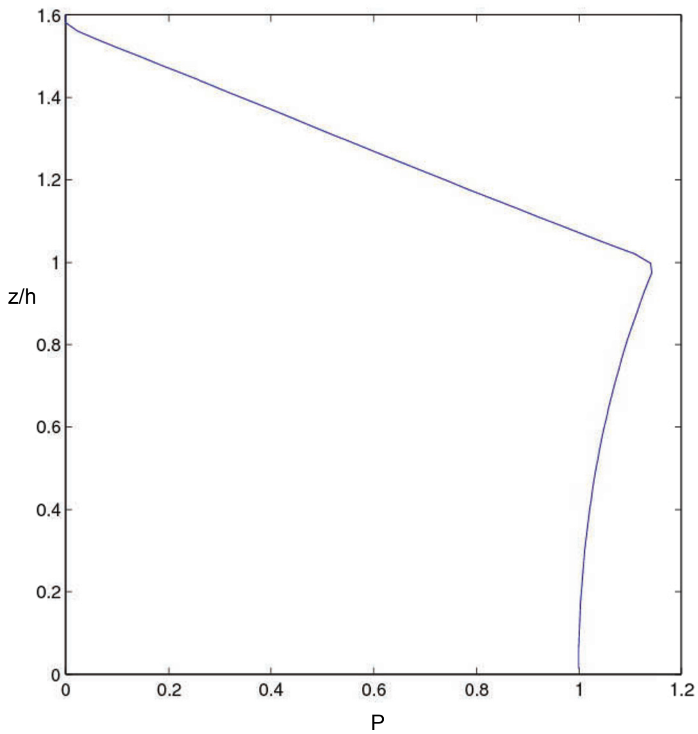

Fig. 7 Numerical solutions for dynamic pressure over the depth in front of the cylinder.

To further ensure that the simulation results are accurate, the time history of the free surface runups at front face of the cylinder and the total force acting on the instrumented cylinder are compared with measured data in Fig. 8 and 9, respectively. Excellent agreement is observed.

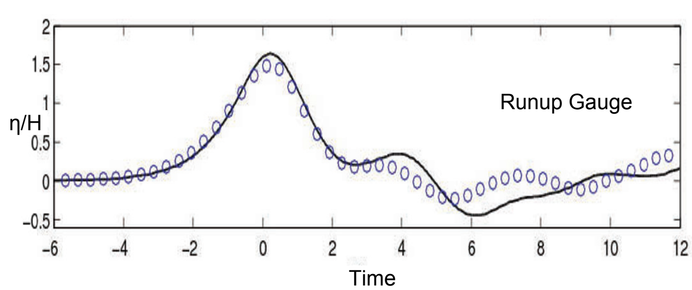

Fig. 8 Free surface runups at front of the cylinder. Circles are measurements and the solid line denotes the numerical results.

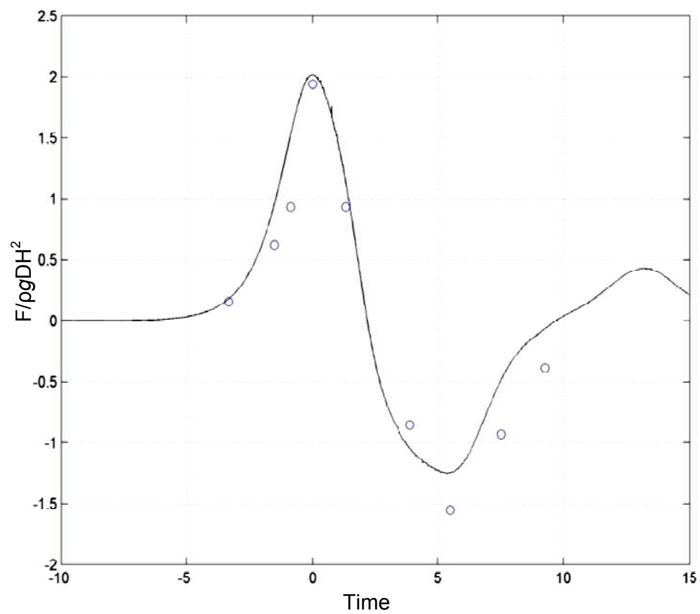

Fig. 9 Total wave force acting on a cylinder for the three-cylinder case. Circles are measurements and the solid line denotes the numerical results.

DISCUSSION ON THE EFFECTS OF MULTIPLE CYLINDERS

Numerical results for the one-cylinder case have also been compared with the experimental data with satisfactory agreement. Similar comparisons for periodic waves interacting with single cylinder can also be found in Mo et al. (2007). In this section, we will show the differences between one-cylinder case and three-cylinder case by using the numerical results.

In Fig. 10 the free surface displacements around the perimeter of the cylinder are shown for both the case of three cylinders and the one cylinder case. It is clear that because of the wave scattering by the two cylinders in front of the instrumented cylinder the leading wave has a smaller wave height and a shorter wavelength. The scattered waves also generated the second wave crest in the case of three cylinders, which are visible along the front face of the cylinder ($0 < \theta < 90°$). Due to the block of the cylinder, the incident solitary wave deforms locally and a trailing wave is created and propagates along the perimeter of the cylinder. This feature is local in the vicinity of a cylinder and occurs in both one-cylinder and three-cylinders cases.

Fig. 11 shows the vertical profiles of the dynamic pressure along the front face of the cylinder for both cases at the phase when the wave crest reaches the cylinder. Over all, the magnitudes of the dynamic pressure are slightly smaller for the 3-cylinder case. Because of the wave scattering, the maximum wave force is also smaller in the 3-cylinder case as shown in Fig. 9 and 12.

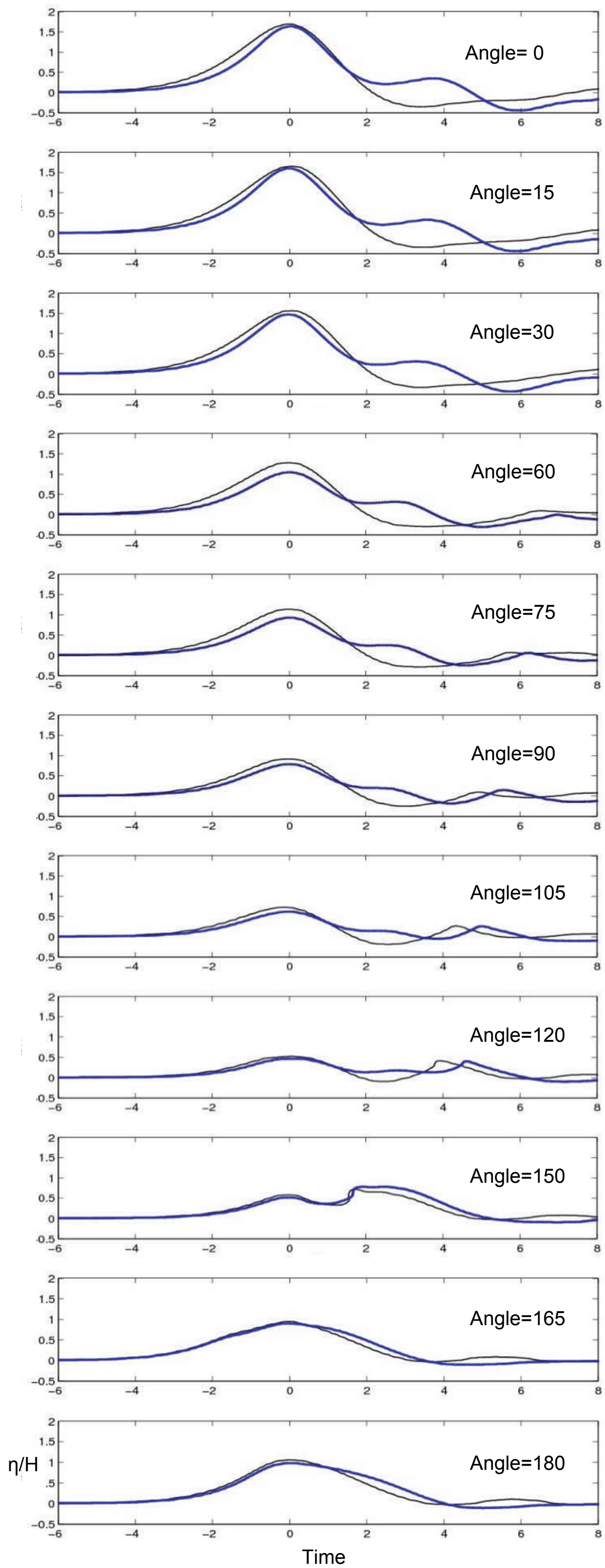

Fig. 10 Free surface displacements around the perimeter of the cylinder. The blue line denotes the case of three cylinders and the black line represents the one cylinder case.

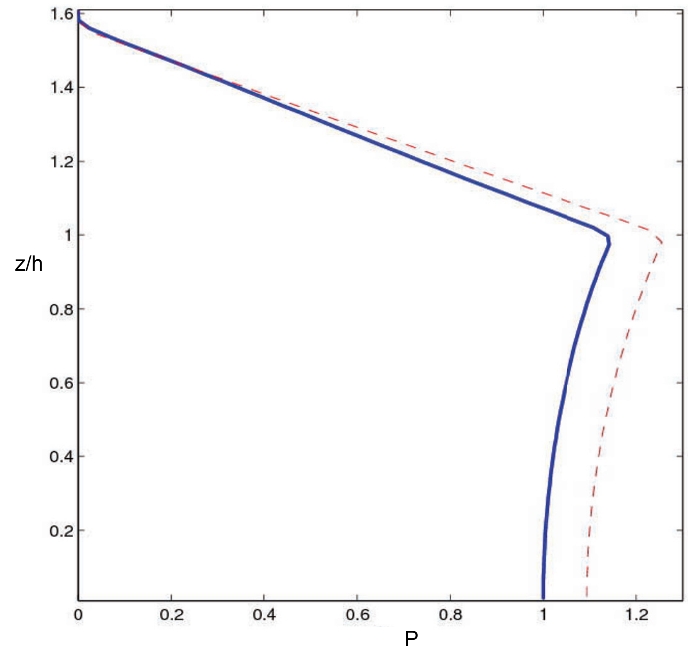

Fig. 11 Vertical profiles of the dynamic pressure along the front face of the cylinder. Solid line represents the 3-cylinder case and the dashed line denotes the 1-cyliner case.

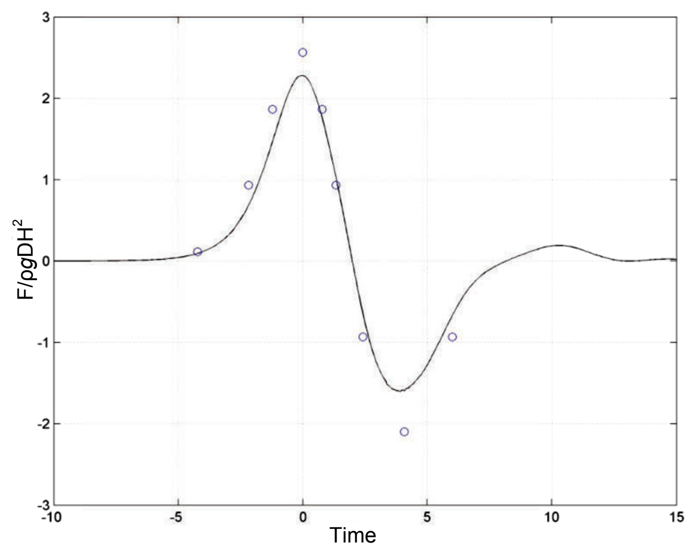

Fig. 12 Total wave force acting on the cylinder in the single cylinder case. Circles are measurements and the solid line denotes the numerical results.

CONCLUDING REMARKS

A 3D numerical model, developed for studying water wave-structure interaction problems, has been tested with experimental data for solitary waves interacting with one cylinder and a group of three vertical cylinders. For the tested cases, waves are non-breaking and turbulence is negligible. The comparisons show that the numerical model is capable of predicting free surface displacement and fluid particle velocity, provided that the correct incident boundary conditions are applied. The relatively less satisfactory agreement is observed in the dynamic pressure on the cylinder. This could be due to the measurement errors.

The numerical model needs to be further validated for breaking waves. More careful measurements for dynamic pressure as well as the forces acting on each cylinder need to be collected.

ACKNOWLEDGEMENT

We would like to acknowledge the support from National Science Foundation of the United States and New York Sea Grant Institute through various research grants to Cornell University. PLF Liu would also acknowledge the support from the Humboldt Foundation in the form of a Humboldt Research Award during the preparation of this paper.

REFERENCES

Christensen, E. D. and Deigaard R., 2001. Large eddy simulation of breaking waves. *Coastal Engng.,* 42, pp.53-86.

Goring, D. J. and Raichlen, F., 1980. The generation of long waves in the laboratory. *Proc. 17th Int. Conf. Coastal Eng.*, ASCE, New York, pp.763-783.

Guyenne, P. and Grilli, S. T., 2006. Numerical study of three-dimensional overturning waves in shallow water. *J. Fluid Mech.,* 547, pp.361-388.

Hirt, C. W. and Nichols, B. D., 1981. Volume of fluid (VOF) method for the dynamics of free boundaries. *J. Comp. Phys*., 39, pp.201-225.

Kim, J., Moin P. and Moser R., 1987. Turbulence statistics in fully developed channel flow at low Reynolds number. *J. Fluid Mech.,* 177, pp.133-166.

Lin, P. and Li, C. W., 2002. A σ-coordinate three-dimensional numerical model for surface wave propagation. *Int. J. Numer. Meth. Fluids*, 38, pp.1048-1068.

Lin, P. and Liu, P. L.-F., 1998. A numerical study of breaking waves in the surf zone. *J. Fluid Mech.*, 359, pp.239-264.

Liu, P. L.-F. Lin, P. Z. and Chang, K. A., 1999. Numerical modeling of wave interaction with porous structures. *J. Wtrwy., Port, Coast., and Oc. Engng*., ASCE, 125(6) pp.322-330.

Liu, P. L.-F. Wu, T.-R. Raichlen, F. Synolakis, C. E. and Borrero, J. C., 2005. Runup and rundown generated by three-dimensional sliding masses. *J. Fluid Mech.,* 536 pp.107-144.

Liu, Y. Xue, M. and Yue, D.K.P., 2001. Computations of fully nonlinear three-dimensional wave-wave and wave-body interactions. Part 2. Nonlinear waves and forces on a body. *J. Fluid Mech.*, 438 , pp.41 – 65.

Mo, W. Irschik, K. Oumeraci, H. and Liu, P. L-F., 2007. A 3D numerical model for computing non-breaking wave forces on slender piles. *J. Eng. Math.,* 58, pp.19-30.

Morison, J. R. O'Brien, M.P. Johnson, J. W. and Schaaf, S. A., 1950. The forces exerted by surface waves on piles. *J. Petroleum Technology*, Petroleum Transctions, AIME, 189, pp.149-154.

Pope, S. B., 2001. *Turbulent flows*. Cambridge University Press.

Pope, S. B., 2004. Ten questions concerning the large-eddy simulation of turbulent flows. *New J. Phys.* 6(35) DOI: 10.1088/1367-2630/6/1/035

Rider, W. J. and Kothe, D. B., 1998. Reconstructing Volume Tracking. *J. Comp. Phys*., 141, pp.112-152.

Sarpkaya, T. and Isaacson, M. St. Q., 1981. *Mechanics of Wave Forces on Offshore Structures*, Van Nostrand Reinold, New York.

Smagorinsky, J., 1963. General circulation experiments with the primitive equations: I. The basic equations. *Mon. Weather Rev. 91*, pp.99-164.

Watanabe, Y. and Saeki, H., 1999. Three-dimensional large eddy simulation of breaking waves. *Coastal Engng*., 41 (3/4), pp.281-301.

WU, T.-R., 2004. A numerical study of three-dimensional breaking waves and turbulence effects. PhD dissertation, Cornell University.

Wu, T-R. and Liu, P. L.-F., 2009a. A large eddy simulation model for tsunami and runup generated by landslides. In: Liu, P. L.-F., Yeh, H. & Synolakis, ed. 2009. *Advances in Coastal and Ocean Engineering,* 10, World Scientific Publishing. Ch.4.

Wu, T.-R. and Liu P. L.-F., 2009b. Numerical study on the three-dimensional dam-break bore interacting with a square cylinder. In: Lynett, P. ed. 2009. *Nonlinear Wave Dynamics*, World Scientific Publishing. Ch.14.

Xue, M. Xu, H. Liu, Y. and Yue, D. K. P., 2001. Computations of fully nonlinear three dimensional wave-wave and wave-body interaction. Part 1. Dynamics of steep three-dimensional waves. *J. Fluid Mech.,* 438, pp.11-39.